Scattering T-matrix theory in wave-vector space for surface-enhanced Raman scattering in clusters of nanoscale spherical metal particles

Karamjeet Arya
Department of Physics, San Jose State University, San Jose, California 95192-0106, USA
(Received 25 August 2006; revised manuscript received 8 September 2006; published 30 November 2006)

Very large enhancements up to 14 orders of magnitude in the Raman cross section from a molecule adsorbed on a single cluster of a few nanoscale metal particles has been reported recently. The enhancement is believed mainly due to the enhanced electric field because of the excitation of the localized surface plasmon modes. We have developed a Green's function theory using scattering *t* matrix approach in the wave-vector space to solve the Maxwell equations for the enhanced field near a spherical metal particle cluster. The advantage of working in the wave-vector space is that one does not need to use complicated translational addition theorem required in the real space as used in earlier calculations. Therefore our theory can be easily extended to any shape or size of the cluster. We consider clusters of two, three, and four spherical particles forming a linear chain, triangle, and square and calculate their localized surface modes. These modes have much more localized field near the cluster compared to those of single metal sphere and are redshifted. We find the enhancement in the Raman cross section can reach up to 10 orders of magnitude due to the resonant excitation of these modes for silver particle clusters and is in a broad frequency range. We also find new results that chainlike clusters of three or more particles have very sharp resonant features that give a dramatic increase in the enhancement near the resonance. The results for gold particle clusters are also presented.

DOI: 10.1103/PhysRevB.74.195438 PACS number(s): 78.66.Bz, 33.20.Fb, 73.20.Mf

I. INTRODUCTION

Surface enhanced Raman spectroscopy was discovered about thirty years back.[1–6] It was found that Raman cross section from a molecule enhances approximately by six orders of magnitude when it is adsorbed on a rough metal (Ag, Au, Cu) surface or on a nanoscale metal particle. This enhancement is now generally believed due to the increased electric field because of the excitation of the localized surface plasmon modes.[5–8] The broadening of the molecular electronic levels due to its interaction with the metal (chemisortion effects) may also contribute some additional enhancement.[4,5,8] Recently, however, very large enhancements up to 14 orders of magnitude in the Raman cross section from rhodamine 6G (R6G) molecule adsorbed on a silver nanoparticle cluster has been reported.[9–18] It is now believed that the excitation of localized surface modes in case of silver nanoparticle cluster may contribute as high as 9–11 orders of magnitude to the enhancement compared to 4–6 orders of magnitude in case of a single spherical nanoparticle.[16,17,19] The additional enhancement of 2–3 orders of magnitude in the Raman cross section from R6G molecule can come from resonance and/or chemisortion effects.

The Raman spectroscopy is widely used in the analysis of the molecular vibrational structure. Since vibrational spectrum is a fingerprint of its molecule it can provide complete identification of a chemical or biological material of interest. However, because of very low cross section (10^{-28}-10^{-30} cm^2/molecule), Raman spectroscopy is mostly limited to analyze large sample volume. For small traces or for the detection of a single molecule, the commonly used spectroscopy technique is fluorescence because of its large cross section ($\sim 10^{-15}$ cm^2/molecule). However, due to such a large enhancement (up to 14 orders) in the cross section in the presence of a silver nanoparticle cluster, the Raman cross section becomes comparable to that of fluorescence. This has lead to a growing interest in the surface enhanced Raman scattering (SERS) phenomena in the last 5–7 yrs to replace fluorescence with Raman spectroscopy for a single chemical or biomolecule (DNA, Protein, etc.) detection.[20–22] Most of the SERS experiments are carried on from silver particle clusters obtained from colloidal solutions. Not all clusters give such a large enhancement. Only a very few clusters termed as "hot spots" and under suitable experimental conditions give large enhancement. To make SERS a viable technique in the detection of a trace of a material or a single molecule, one needs to analyze what shape or size of the nanoparticle cluster can give the maximum enhancement. Therefore, instead of using self-arranged particle clusters from colloidal solutions one can engineer a cluster with a specific shape and size for the maximum enhancement.

The electric field from a single spherical metal particle can be easily calculated as exact solutions of Maxwell equations for a dielectric sphere are well known.[7,23] However, for a cluster of two or more spherical particles, Maxwell equations can be solved only approximately in the nonretardation limit.[24–28] Inoue *et al.*[29] developed a Green's function approach to calculate the electric field near a cluster that includes multiple scattering of spherical waves between the spherical particles forming the cluster. The spherical waves are expressed in terms of vector spherical harmonics with respect to the center of a respective sphere. Their approach is based on including multiple scattering in the real space. Therefore one needs to use translational addition theorem for the coordinate transformation of the vector spherical harmonics between the centers of the spheres in the cluster.[30–32] They have thus calculated the enhanced electric field near a simple cluster of few spherical particles. This approach is quite involved and is not simple to extend to different shape or size of the cluster.

In this paper, we have developed a Green's function theory using scattering t matrix in the Fourier (wave-vector) space. It has been earlier used to include multiple scattering of electromagnetic (em) waves from a random distribution of dielectric spheres.[33–35] In the wave-vector ($\vec{k}$) space, one does not need any coordinate transformation for the vector spherical harmonics. It simply adds an exponential factor $e^{i\vec{k}\cdot\vec{R}_\alpha}$ for each sphere α in the cluster where $\vec{R}_\alpha$ is the position vector of its center. This can be handled easily in the calculations compared to the use of translational addition theorem. This makes our approach simpler and thus can be easily extended to determine the enhanced field near a cluster of any shape or size.

In Sec. II, we discuss the Green's function formulation based on the scattering T matrix for the cluster and obtain a general expression for the electric field at any point. We then discuss the multiple scattering between the spheres and obtain an integral equation for the scattering T matrix for the cluster in terms of the single sphere scattering matrix. In the Fourier space and in the angular momentum representation, the integral equation reduces to a matrix equation that can be solved numerically. We would like to mention that the definition used for vector spherical harmonics by various authors in the literature is not consistent at least with respect to the prefactor as in usual spherical harmonics $y_{lm}(\theta,\phi)$.[23,29,33,36] We, however, use the definition consistent with that used in Refs. 23 and 36–38. Furthermore, we find the treatment of vector spherical harmonics in Ref. 36 in terms of coupling of photon orbital and spin angular momentum through Clebsch-Gorden coefficients very useful and convenient to derive some of the relations involving this analysis. In the Appendix, we have given this definition and derive some of the useful results analytically using this definition.

In Sec. III, we give numerical results for the enhancement in the electric field intensity and in the Raman cross section in the presence of a metal particle cluster. We consider two particles cluster in the shape of a dimer and three and four particles forming a linear chain, triangular, and square shape clusters. For two particles cluster we first derive analytically the results obtained earlier[24–26] in the dipole approximation by including only lowest partial wave ($l=1$) contribution in our theory. Our theory reproduces exactly the same results, for example, for the number of modes, their excitation energies and their electric field strength. However, when higher partial waves are included in our theory, we find their field strength enhanced (more localized modes) and also a shift towards longer wavelength. In addition, new modes appear corresponding to higher partial waves and those can also be excited optically. We also find that the enhancement in Raman cross section can reach up to 10 orders of magnitude. The large enhancement is usually found when the molecule is lying trapped between the particles or very close to the cavity. Similar results are also obtained for three and four particle clusters with maximum enhancements in Raman cross section reaching up to 10 orders of magnitude. However, for linear chain of three or more particles, we find important new results where the enhancement in Raman cross section drops dramatically near the resonant peak. These sharp resonant features indicate the existence of very localized modes for a chain and are the result of interference effects of higher partial waves included in our theory. We also consider clusters of gold nanoparticles. However, the enhancement in Raman cross section is between 7–8 orders of magnitude only because of large imaginary parts of the dielectric function of gold. We conclude these results in Sec. IV.

II. GREEN'S FUNCTION FORMULATION

A. General expression

We consider a single cluster of an arbitrary number of spherical metal particles with the same or different radii embedded in a host medium of dielectric constant ε_0. These particles may be touching each other but do not overlap. The electric field $\vec{E}(\vec{r},\omega)$ at any point then satisfies the Maxwell equation

$$-\vec{\nabla}\times\vec{\nabla}\times\vec{E}(\vec{r},\omega)+k^2\varepsilon(\vec{r},\omega)\vec{E}(\vec{r},\omega)=4\pi\left(\frac{-i\omega}{c^2}\right)\vec{j}^0(\vec{r},\omega), \tag{2.1}$$

where $k^2=\varepsilon_0\omega^2/c^2$ and $\vec{j}^0(\vec{r},\omega)$ is the current source corresponding to the incident field of frequency ω. $\varepsilon(\vec{r},\omega)$ is the scaled dielectric function equal to 1 for $\vec{r}$ in the host medium and $\varepsilon(\omega)/\varepsilon_0$ for $\vec{r}$ within any metal sphere. We define the photon Green's function $\overleftrightarrow{d}$ as the solution of Maxwell equation

$$-\vec{\nabla}\times\vec{\nabla}\times\overleftrightarrow{d}(\vec{r},\vec{r}'\omega)+k^2\varepsilon(\vec{r},\omega)\overleftrightarrow{d}(\vec{r},\vec{r}'\omega)=4\pi\delta(\vec{r}-\vec{r}')\overleftrightarrow{I}, \tag{2.2}$$

where $\overleftrightarrow{I}$ is a unit dyadic. From Eqs. (2.1) and (2.2) one can write

$$\vec{E}(\vec{r},\omega)=\left(\frac{-i\omega}{c^2}\right)\int d^3r'\overleftrightarrow{d}(\vec{r},\vec{r}',\omega)\cdot\vec{j}^0(\vec{r}',\omega). \tag{2.3}$$

We now define the scattering $\overleftrightarrow{T}$ matrix for the cluster as

$$\overleftrightarrow{d}(\vec{r},\vec{r}',\omega)=\overleftrightarrow{d}^0(\vec{r},\vec{r}',\omega)+\int d^3r''d^3r''' \times\overleftrightarrow{d}^0(\vec{r},\vec{r}'',\omega)\,.\,\overleftrightarrow{T}(\vec{r}'',\vec{r}''',\omega)\cdot\overleftrightarrow{d}^0(\vec{r}''',\vec{r}',\omega), \tag{2.4}$$

where $\overleftrightarrow{d}^0(\vec{r},\vec{r}',\omega)$ is the photon Green's function for the host medium [replace $\varepsilon(\vec{r},\omega)$ by 1 in Eq. (2.2)]. Using Eq. (2.4) in Eq. (2.3) we find

$$\vec{E}(\vec{r},\omega) = \vec{E}_{inc}(\vec{r},\omega) + \int d^3r' d^3r'' \times \vec{\vec{d}}^0(\vec{r},\vec{r}',\omega) \cdot \vec{\vec{T}}(\vec{r}',\vec{r}'',\omega) \cdot \vec{E}_{inc}(\vec{r}'',\omega), \quad (2.5)$$

where $\vec{E}_{inc}(\vec{r},\omega)$ is the incident field.

It is convenient to work in spherical polar coordinates because of the spherical geometry of the scattering particles in the cluster. Therefore we write the expression for the host Green's function $\vec{\vec{d}}^0$ also in these coordinates. This can be easily done since eigensolutions of the Maxwell equation for the host medium are well known in spherical polar coordinates. For example[29]

$$\vec{\vec{d}}^0(\vec{r},\vec{r}',\omega) = -4\pi ik \sum_{lm\sigma} \vec{A}_{klm\sigma}(\vec{r}) \vec{A}^*_{klm\sigma}(\vec{r}'), \quad r \neq r'$$

$$= \frac{4\pi}{k^2} \delta(\vec{r}-\vec{r}') \vec{\vec{I}}, \quad r = r', \quad (2.6)$$

where $\vec{A}_{klm\sigma}(\vec{r})$ are the two electric ($\sigma=1$) and magnetic ($\sigma=2$) transverse eigenmodes of the homogeneous Maxwell equation (2.1) with $\varepsilon(\vec{r},\omega)=1$. These are given as[23]

$$\vec{A}_{klm1}(\vec{r}) = \frac{i}{k} \vec{\nabla} \times [f_l(kr) \vec{X}_{lm}(\Omega)]$$

$$= \frac{i}{k} \left[\frac{1}{r} \frac{\partial}{\partial r} (r f_l(kr)) \hat{r} \times \vec{X}_{lm}(\Omega) + i\sqrt{l(l+1)} \frac{f_l(kr)}{r} y_{lm}(\Omega) \hat{r} \right], \quad (2.7)$$

$$\vec{A}_{klm2}(\vec{r}) = f_l(kr) \vec{X}_{lm}(\Omega), \quad (2.8)$$

$$\vec{X}_{lm}(\Omega) = \frac{1}{\sqrt{l(l+1)}} \vec{L} y_{lm}(\Omega), \quad (2.9)$$

where $\vec{L} = -i\vec{r} \times \vec{\nabla}$ is the angular momentum operator and $f_l(r)$ is the spherical Bessel function $j_l(r)$ or the Henkel function $h_l^{(1)}(r)$ of the first kind depending on whether r includes the origin or not. Also $y_{lm}(\Omega)$ are the usual spherical harmonics where $\Omega=(\theta,\phi)$ are the polar angles of $\vec{r}$. Note that $\vec{X}_{lm}(\Omega)$, hence $\vec{A}_{klm\sigma}(\vec{r})$ are equal to zero for $l=0$. One can show this from Eq. (2.9) or from Eq. (A6). Therefore, in the following, the summation includes terms only for $l \geq 1$.

The solution of Eq. (2.5) has been discussed earlier in Ref. 29 in the real space using the translational addition theorem. We, however, solve it in the Fourier (wave-vector) space. We find our treatment in the Fourier space is simpler and easy to extend to any shape or size of the cluster. We define the Fourier transformations as

$$\vec{A}_{klm\sigma}(\vec{r}) = \int \frac{d^3Q}{(2\pi)^3} e^{i\vec{Q}\cdot\vec{r}} \vec{A}_{klm\sigma}(\vec{Q}), \quad (2.10)$$

$$\vec{\vec{T}}(\vec{r},\vec{r}',\omega) = \int \frac{d^3k}{(2\pi)^3} \frac{d^3k'}{(2\pi)^3} e^{i(\vec{k}\cdot\vec{r}-\vec{k}'\cdot r')} \vec{\vec{T}}(\vec{k},\vec{k}',\omega). \quad (2.11)$$

Using Eq. (2.6) and these Fourier transformations, one can rewrite Eq. (2.5) as

$$\vec{E}(\vec{r},\omega) = \vec{E}_{inc}(\vec{r},\omega) - 4\pi ik \sum_{lm\sigma} \vec{A}_{klm\sigma}(\vec{r}) \int \frac{d^3k_1}{(2\pi)^3} \vec{A}^*_{klm\sigma}(\vec{k}_1) \cdot \vec{\vec{T}}(\vec{k}_1,\vec{k},\omega) \cdot \vec{E}_{inc}(\vec{k},\omega), \quad (2.12)$$

where we have assumed the incident field

$$\vec{E}_{inc}(\vec{r},\omega) = \vec{E}_{inc}(\vec{k},\omega) e^{i\vec{k}\cdot\vec{r}}, \quad (2.13)$$

as a single plane wave of wave vector $\vec{k}$ and frequency ω. The second term on the right hand side of Eq. (2.12) thus describes the scattered field by the cluster.

The expressions for $\vec{A}_{klm\sigma}(\vec{r})$ in spherical polar coordinates [Eqs. (2.7)–(2.9)] are quite involved. As a result, most of the earlier calculations are limited to the scattering problem from a single dielectric sphere. We, however, find it convenient to write these functions in terms of vector spherical harmonics $\vec{V}_{lLm}(\Omega)$ or $\vec{Y}_{lm\sigma}(\Omega)$. These functions have been discussed briefly in Refs. 36 and 38 and are obtained from the addition of an orbital and spin angular momentum of a photon in terms of the Clebch-Gorden (CG) coefficients. In the Appendix, we have given the definitions of these vector spherical harmonics from Ref. 36 and also expressed $\vec{A}_{klm\sigma}(\vec{r})$ in terms of these functions. We find them very useful in deriving some of the results analytically. We will need them for the scattering problem from a cluster of spherical particles in the following section. These are also helpful in the numerical calculations of the enhanced electric field. For example, using these relations and using the orthogonality relation for the spherical Bessel functions:

$$\int_0^\infty f_l(kr) f_l(k'r) r^2 dr = \frac{\pi}{2k^2} \delta(k-k'), \quad (2.14)$$

one can derive the Fourier transformations of $\vec{A}_{klm\sigma}(\vec{r})$ from Eqs. (2.7)–(2.9) as (see the Appendix)

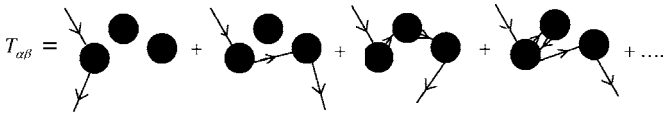

FIG. 1. Schematic picture of multiple scattering of a photon from the dielectric spheres in a three-particle cluster.

$$\vec{A}_{klm\sigma}(\vec{Q}) = 4\pi(-i)^l(-1)^\sigma \vec{Y}_{lm\sigma}(\Omega_Q)\frac{\pi}{2k^2}\delta(k-Q), \tag{2.15}$$

where

$$\vec{Y}_{lm1}(\Omega_k) = \hat{k}\times\vec{X}_{lm}(\Omega_k), \tag{2.16}$$

$$\vec{Y}_{lm2}(\Omega_k) = \vec{X}_{lm}(\Omega_k), \tag{2.17}$$

are the vector spherical harmonics.[36–38] Some of the other useful results have also been derived in terms of vector spherical harmonic in the Appendix.

B. Multiple scattering

We now discuss the scattering $\overleftrightarrow{T}$ matrix of the cluster in the framework of the multiple scattering theory. Let $\overleftrightarrow{t}_\alpha(\vec{r}-\vec{R}_\alpha,\vec{r}'-\vec{R}_\alpha,\omega)$ denotes the scattering matrix of the single spherical particle centered at $\vec{R}_\alpha$. Then the scattering $\overleftrightarrow{T}$ matrix of the cluster can be written as a series expansion in terms of $\overleftrightarrow{t}_\alpha$ as[33,34]

$$\overleftrightarrow{T}(\vec{r},\vec{r}',\omega) = \sum_{\alpha,\beta}\overleftrightarrow{T}_{\alpha\beta}(\vec{r}-\vec{R}_\alpha,\vec{r}'-\vec{R}_\beta,\omega), \tag{2.18}$$

$$\overleftrightarrow{T}_{\alpha\beta} = \overleftrightarrow{t}_\alpha\delta_{\alpha\beta} + \overleftrightarrow{t}_\alpha\cdot\overleftrightarrow{d}^0\cdot\overleftrightarrow{t}_\beta g(\alpha|\beta) + \sum_\gamma \overleftrightarrow{t}_\alpha\cdot\overleftrightarrow{d}^0\cdot\overleftrightarrow{t}_\gamma\cdot g(\alpha|\gamma)\overleftrightarrow{d}^0\cdot\overleftrightarrow{t}_\beta g(\gamma|\beta) + \cdots. \tag{2.19}$$

In Eq. (2.19), we have suppressed the explicit dependence on $\vec{r},\vec{r}_1,\ldots,\vec{r}'$ and ω. Also $\overleftrightarrow{T}_{\alpha\beta}$ describes all scattering possibilities from sphere β to α due to multiple scattering within the cluster. However, consecutive multiple scattering from the same sphere is not allowed. This is included in Eq. (2.19) by the function $g(\alpha|\beta)=0$ for $\alpha=\beta$ and $=1$ otherwise. This is shown schematically in Fig. 1. The series expansion in Eq. (2.19) can be expressed by an integral equation as

$$\overleftrightarrow{T}_{\alpha\beta}(\vec{r}-\vec{R}_\alpha,\vec{r}'-\vec{R}_\beta,\omega) = \overleftrightarrow{t}_\alpha(\vec{r}-\vec{R}_\alpha,\vec{r}'-\vec{R}_\alpha,\omega)\delta_{\alpha\beta} + \sum_\gamma\int d^3r_1 d^3r_2 \overleftrightarrow{t}_\alpha(\vec{r}-\vec{R}_\alpha,\vec{r}_1-\vec{R}_\alpha,\omega)\cdot\overleftrightarrow{d}^0(\vec{r}_1,\vec{r}_2,\omega)\cdot g(\alpha|\gamma)\overleftrightarrow{T}_{\gamma\beta}(\vec{r}_2-\vec{R}_\gamma,\vec{r}'-\vec{R}_\beta,\omega). \tag{2.20}$$

Using the Fourier transformations as defined in Eq. (2.11) for $\overleftrightarrow{t}_\alpha$ and $\overleftrightarrow{T}_{\alpha\beta}$, one can show that

$$\overleftrightarrow{T}(\vec{k},\vec{k}',\omega) = \sum_{\alpha,\beta}\overleftrightarrow{T}_{\alpha\beta}(\vec{k},\vec{k}',\omega)e^{-i(\vec{k}\cdot\vec{R}_\alpha-\vec{k}'\cdot\vec{R}_\beta)}, \tag{2.21}$$

where in the Fourier space the integral equation (2.20) reduces to the following integral equation for $\overleftrightarrow{T}_{\alpha\beta}(\vec{k},\vec{k}',\omega)$:

$$\overleftrightarrow{T}_{\alpha\beta}(\vec{k},\vec{k}',\omega) = \overleftrightarrow{t}(\vec{k},\vec{k}',\omega)\delta_{\alpha\beta} + \sum_\gamma\int\frac{d^3k_1}{(2\pi)^3}\overleftrightarrow{t}(\vec{k},\vec{k}_1,\omega)\cdot\overleftrightarrow{d}^0(k_1,\omega)\cdot e^{i\vec{k}_1\cdot(\vec{R}_\alpha-\vec{R}_\gamma)}g(\alpha|\gamma)\overleftrightarrow{T}_{\gamma\beta}(\vec{k}_1,\vec{k}',\omega). \tag{2.22}$$

In Eq. (2.22), $\overleftrightarrow{d}^0(k_1,\omega)$ is the Fourier transform of the host medium Green's function. Using translational symmetry of the host medium, that is, $\overleftrightarrow{d}^0(\vec{r}_1,\vec{r}_2,\omega)=\overleftrightarrow{d}^0(\vec{r}_1-\vec{r}_2,\omega)$ and Eq. (2.15), one can easily obtain its expression from Eq. (2.6) as

$$\overleftrightarrow{d}^0(k_1,\omega) = -i\frac{2\pi^2}{k}\delta(k-k_1)\overleftrightarrow{I}. \tag{2.23}$$

We now discuss the solution of the integral equation (2.22). Since solutions of Maxwell equations for a single dielectric sphere are well known in spherical polar coordinates, one can easily derive the expression for a single sphere t matrix using the vector spherical harmonics as (see the Appendix)

$$\overleftrightarrow{t}_\alpha(\vec{k},\vec{k}',\omega) = \frac{4\pi i}{k}\sum_{lm\sigma}\vec{Y}_{lm\sigma}(\Omega_k)c_{kl\sigma\alpha}\vec{Y}^*_{lm\sigma}(\Omega_{k'}), \tag{2.24}$$

where $|\vec{k}|=|\vec{k}'|=\sqrt{\varepsilon_0}\omega/c$. $c_{kl\sigma\alpha}$ are the Mie scattering coefficients of a spherical wave $\vec{A}_{klm\sigma}(\vec{r})$ from a dielectric sphere of radius $R(\alpha)$ and dielectric constant $\varepsilon(\omega)$. These are given as[23,39]

$$c_{kl1\alpha} = \frac{-\varepsilon(\omega) j_l[k_i R(\alpha)]\{kR(\alpha) j_l[kR(\alpha)]\}' + j_l[kR(\alpha)]\{k_i R(\alpha) j_l[k_i R(\alpha)]\}'}{\varepsilon(\omega) j_l[kR(\alpha)]\{kR(\alpha) h_l^{(1)}[kR(\alpha)]\}' + h_l^{(1)}[kR(\alpha)]\{k_i R(\alpha) j_l[k_i R(\alpha)]\}'}, \tag{2.25}$$

$$c_{kl2\alpha} = \frac{j_l[k_i R(\alpha)]\{kR(\alpha) j_l[kR(\alpha)]\}' + j_l[kR(\alpha)]\{k_i R(\alpha) j_l[k_i R(\alpha)]\}'}{h_l^{(1)}[kR(\alpha)]\{k_i R(\alpha) j_l[k_i R(\alpha)]\}' + j_l[k_i R(\alpha)]\{kR(\alpha) h_l^{(1)}[kR(\alpha)]\}'}, \tag{2.26}$$

where $k_i = \sqrt{\varepsilon(\omega)}k$. The prime in Eqs. (2.25) and (2.26) denotes the derivative of the term within the brackets with respect to the arguments of the spherical Bessel j_l or Henkel function $h_l^{(1)}$.

Equation (2.22) is a tensor integral equation. However, because of the separable nature of the tensor $\ddot{t}_\alpha(\vec{k},\vec{k}',\omega)$ [see Eq. (2.24)], this integral equation can be reduced to a scalar matrix equation in the angular momentum representation. For example, writing some of the terms in the series expansion of Eq. (2.22), one can show that $\ddot{\vec{T}}_{\alpha\beta}(\vec{k},\vec{k}',\omega)$ is of the form

$$\ddot{\vec{T}}_{\alpha\beta}(\vec{k},\vec{k}',\omega) = \frac{4\pi i}{k} \sum_{lm\sigma,l'm'\sigma'} i^{l'-l}(-1)^{\sigma'-\sigma} \vec{Y}_{lm\sigma}(\Omega_k) c_{kl\sigma\alpha} Q(lm\sigma\alpha|l'm'\sigma'\beta) Y^*_{l'm'\sigma'}(\Omega_{k'}), \tag{2.27}$$

where the scalar function $Q(lm\sigma\alpha|l'm'\sigma'\beta)$ satisfies the following scalar matrix equation

$$Q(lm\sigma\alpha|l'm'\sigma'\beta) = \delta_{ll'}\delta_{mm'}\delta_{\sigma\sigma'}\delta_{\alpha\beta} + \sum_{l_1 m_1 \sigma_1 \gamma} B(lm\sigma R_\alpha|l_1 m_1 \sigma_1 R_\gamma) c_{kl_1\sigma_1\gamma} Q(l_1 m_1 \sigma_1 \gamma|l'm'\sigma'\beta), \tag{2.28}$$

and the matrix B is given as

$$B(lm\sigma R_\alpha|l'm'\sigma' R_\gamma) = i^{l-l'}(-1)^{\sigma-\sigma'} \int d\Omega_k \vec{Y}^*_{lm\sigma}(\Omega_k) \cdot \vec{Y}_{l'm'\sigma'}(\Omega_k) e^{-i\vec{k}\cdot(\vec{R}_\gamma - \vec{R}_\alpha)} g(\alpha|\gamma). \tag{2.29}$$

The solution of Eq. (2.28) can then be written in the matrix notation as

$$Q = [I - Bc]^{-1}. \tag{2.30}$$

The angular integration in Eq. (2.29) can be simplified by expanding the exponential function $e^{-i\vec{k}\cdot(\vec{R}_\gamma - \vec{R}_\alpha)}$ for $\vec{R}_\gamma \neq \vec{R}_\alpha$ in terms of Henkel function of first kind as

$$e^{-i\vec{k}\cdot(\vec{R}_\gamma - \vec{R}_\alpha)} = 4\pi \sum_{l_1 m_1} (-i)^{l_1} h^{(1)}_{l_1}(kR_{\gamma\alpha}) y_{l_1 m_1}(\Omega_k) y^*_{l_1 m_1}(\Omega_{R_{\gamma\alpha}}), \tag{2.31}$$

where $\vec{R}_{\gamma\alpha} = \vec{R}_\gamma - \vec{R}_\alpha$. Therefore, one has

$$B(lm\sigma R_\alpha|l'm'\sigma' R_\gamma) = 4\pi \sum_{l_1 m_1} i^{l-l'-l_1}(-1)^{\sigma-\sigma'} h^{(1)}_{l_1}(kR_{\gamma\alpha}) \times y^*_{l_1 m_1}(\Omega_{R_{\gamma\alpha}}) g(\alpha|\gamma) C^{l_1 m_1}_{lm\sigma,l'm'\sigma'}, \tag{2.32}$$

where

$$C^{l_1 m_1}_{lm\sigma,l'm'\sigma'} = \int d\Omega \vec{Y}^*_{lm\sigma}(\Omega) \cdot \vec{Y}_{l'm'\sigma'}(\Omega) y_{l_1 m_1}(\Omega) \tag{2.33}$$

are Gaunt coefficients. One can calculate them by expressing $\vec{Y}_{lm\sigma}(\Omega)$ in terms of the usual spherical harmonics [Eqs. (A5) and (A6)]. This leads to the addition of three angular momentums. The angular integration can then be carried out in terms of the CG coefficients. We have given these expressions in the Appendix, which are easy to use for numerical purposes.

Thus using Eqs. (2.15), (2.21), and (2.27) in Eq. (2.12), we find

$$\vec{E}(\vec{r},\omega) = \vec{E}_{inc}(\vec{r},\omega) + \sum_{lm\sigma} \vec{A}_{klm\sigma}(\vec{r}) \sum_{l_1 m_1 \sigma_1 l'm'\sigma'\alpha\beta} \tilde{B}(lm\sigma 0|l_1 m_1 \sigma_1 R_\alpha) c_{kl_1\sigma_1} Q(l_1 m_1 \sigma_1 \alpha|l'm'\sigma'\beta) a^{inc}_{l'm'\sigma'}(\vec{k}) e^{i\vec{k}\cdot\vec{R}_\beta}, \tag{2.34}$$

where the matrix $\tilde{B}$ in Eq. (2.34) is essentially the same as the matrix B in Eq. (2.29) except one of the R vector is zero. In writing Eq. (2.34), we have used the expansion of the incident plane wave in to vector spherical harmonics as

$$\vec{E}_{inc}(\vec{k},\omega)e^{i\vec{k}\cdot\vec{r}} = \sum_{lm\sigma} a^{inc}_{lm\sigma}(\vec{k})\vec{A}_{klm\sigma}(\vec{r}), \tag{2.35}$$

where $a^{inc}_{lm\sigma}(\vec{k})$ are the expansion coefficients. These can be determined using the Fourier transformations on both sides of Eq. (2.35) and using Eq. (2.15) as (see the Appendix)

$$a^{inc}_{lm\sigma}(\vec{k}) = 4\pi i^l(-1)^\sigma \vec{E}^{inc}(\vec{k},\omega)\cdot\vec{Y}^*_{lm\sigma}(\Omega_k). \tag{2.36}$$

In Eq. (2.34), the second term on the right hand side corresponds to the scattered field $\vec{E}_{sc}(\vec{r},\omega)$ from the cluster. Similar to Eq. (2.35), one can also write

$$\vec{E}_{sc}(\vec{r},\omega) = \sum_{lm\sigma} a^{sc}_{lm\sigma}(\vec{k})\vec{A}_{klm\sigma}(\vec{r}), \tag{2.37}$$

where

$$a^{sc}_{lm\sigma}(\vec{k}) = \sum_{l_1m_1\sigma_1l'm'\sigma'\alpha\beta} \tilde{B}(lm\sigma 0|l_1m_1\sigma_1R_\alpha)c_{kl_1\sigma_1} \times Q(l_1m_1\sigma_1\alpha|l'm'\sigma'\beta)a^{inc}_{l'm'\sigma'}(\vec{k})e^{i\vec{k}\cdot\vec{R}_\beta}, \tag{2.38}$$

are the scattering coefficients of a spherical wave $\vec{A}_{klm\sigma}(\vec{r})$ by the cluster. Thus the total field $\vec{E}(\vec{r},\omega)=\vec{E}_{inc}(\vec{r},\omega)+\vec{E}_{sc}(\vec{r},\omega)$ at any point $\vec{r}$ can be written as

$$\vec{E}(\vec{r},\omega) = \sum_{lm\sigma}[a^{inc}_{lm\sigma}(\vec{k}) + a^{sc}_{lm\sigma}(\vec{k})]\vec{A}_{klm\sigma}(\vec{r}). \tag{2.39}$$

In the derivation of Eq. (2.34), one can choose any origin for the spherical polar coordinate system. In Ref. 29, similar calculations are carried on in real space where the origin is taken as the center of one of the spheres. Therefore, one needs a coordinate transformation for the vector spherical harmonics for another sphere with respect to the first one. This makes the calculations very involved. However, in the Fourier wave-vector space, it just corresponds to an additional exponential factor of the type $e^{-i\vec{k}\cdot(\vec{R}_\gamma-\vec{R}_\alpha)}$ in B matrix [Eq. (2.29)], which can be handled easily. For simplification of numerical work, we chose the origin to be the point where the field is calculated, that is, outside any sphere. For example, in SERS it can be the position of the molecule. In this case, $\vec{A}_{klm\sigma}(\vec{r})$ in Eq. (2.39) will contain only $j_l(r)$ and for $r\to 0$, only $l=1$ and $\sigma=1$ terms contribute. Note that $l=0$ term is not allowed in the summation. One can also show that from Eqs. (2.7) or (A8)that $\vec{A}_{k1m1}(\vec{r}\to 0)=-\hat{e}_m/\sqrt{6\pi}$ where the unit vectors $\hat{e}_m$ are defined in Eq. (A2). Thus from Eq. (2.39), we have

$$\vec{E}(\vec{r}\to 0,\omega) = -\frac{1}{\sqrt{6\pi}}\sum_{m=-1}^{1}[a^{inc}_{1m1}(\vec{k}) + a^{sc}_{1m1}(\vec{k})]\hat{e}_m. \tag{2.40}$$

We now define the enhancement factor in the electric field intensity in the presence of the cluster compared to the intensity at the same point in the host medium as

$$F(\vec{k},\omega) = \left|\frac{\vec{E}(\vec{r},\omega)}{\vec{E}_{inc}(\vec{r},\omega)}\right|^2 = \frac{\sum_{m=-1}^{1}\left|a^{inc}_{1m1}(\vec{k}) + a^{sc}_{1m1}(\vec{k})\right|^2}{\sum_{m=-1}^{1}\left|a^{inc}_{1m1}(\vec{k})\right|^2}. \tag{2.41}$$

One can also discuss the contribution due to the enhanced electric field in the Raman cross section from a molecule adsorbed on a metal nanoparticle cluster. The Raman cross section σ from a free molecule has the expression of the type

$$\sigma^{\text{Raman}}_{\text{mole}} \propto \left|\frac{\langle g,1|\vec{r}\cdot\vec{E}^0(\vec{r},\omega_s)|\langle m,1\rangle\langle m,1|H_{el\text{-}vib}|m,0\rangle\langle m,0|\vec{r}\cdot\vec{E}^0(\vec{r},\omega_i)|g,0\rangle}{(E_m-E_g-\hbar\omega_s)(E_m-E_g-\hbar\omega_i)}\right|^2. \tag{2.42}$$

In Eq. (2.42), $|g,\nu\rangle$ and $|m,\nu\rangle$ are the free molecule states where g and m correspond to the ground and excited electronic states with energies E_g and E_m, respectively, and $\nu=0,1$ corresponds to the vibrational states of the molecule. Also $H_{el\text{-}vib}$ is the electron-vibration interaction in the molecule and $\hbar\omega_i$ and $\hbar\omega_s$ are the incident and Raman scattered photon frequencies, respectively. $\vec{E}^0(\vec{r},\omega_i)$ and $\vec{E}^0(\vec{r},\omega_s)$ are the dipole electric fields seen by the molecule in the free space. However, if the molecule is lying close to the cluster, it will see the enhanced field due to the multiple scattering from the cluster. In the SERS, both fields at incident and Raman scattered frequencies (ω_i, ω_s) will be enhanced. Therefore, the enhancement in the Raman cross section can be written as

$$\frac{\sigma^{SERS}}{\sigma^{free}} = \left|\frac{\vec{E}(\vec{r},\omega_i)}{\vec{E}^0_{inc}(\vec{r},\omega_i)}\right|^2\left|\frac{\vec{E}(\vec{r},\omega_s)}{\vec{E}^0_{inc}(\vec{r},\omega_s)}\right|^2 = F(\vec{k}_i,\omega_i)F(\vec{k}_s,\omega_s), \tag{2.43}$$

where $\vec{k}_i$ and $\vec{k}_s$ are the incident and scattered photon wave vectors, respectively.

III. NUMERICAL RESULTS AND DISCUSSIONS

We now give numerical results for the enhancement in the electric field intensity and in the Raman cross section from a molecule due to the presence of a cluster calculated from Eqs. (2.14) and (2.43), respectively. We have considered clusters of both silver and gold nanoparticles. The dielectric constant $\varepsilon(\omega)$ of silver and gold is taken from the experimental work of Johnson and Christy.[40] This data in terms of wavelength is also given in the Appendix of Ref. 41. The host dielectric constant $\varepsilon_0=1$. We have considered clusters made of two, three, and four spherical particles arranged in different shapes as linear chain, triangular, and square. As discussed in the previous section, we assume the position of the molecule as the origin of the coordinate system. This is not a required condition, however, it reduces the computational time considerably without any approximation. Therefore, in our calculations, the vector $\vec{R}_\alpha$ in Eq. (2.29) corresponds to the coordinates of the center of sphere α with respect to this origin (molecule).

One should note that there are three factors contributing to the SERS enhancement: (i) The resonant excitation of the localized modes of the cluster. In our theory, these modes correspond to the poles of the scattering T-matrix those are also the poles of the matrix Q [see Eqs. (2.27) and (2.30)]. The resonant position of these modes depends on the size and shape of the cluster. (ii) The probability of the excitation of these modes by the incident (scattered) photon. This may depend, for example, on the polarization and wavelength of the photon and all these modes may not be optical active. (iii) The electric field strength of the localized mode at the position of the molecule. The electric field of these modes is highly localized. Therefore, large enhancements are possible only if the molecule lies very close to the cluster. We now discuss clusters of two and more than two spherical particles separately.

A. Two particles cluster (dimer)

The localized modes of a dimer have been discussed earlier in Refs. 24–26 in the dipole approximation ($l=1$). The SERS enhancement has also been calculated in Refs. 16, 17, and 29 using multiple scattering approaches in the real space. Our theory using multiple scattering in wave-vector space also gives similar results. For example, in Fig. 2, we consider cluster of two silver spheres each of radius 20 nm. The molecule is assumed to be in the middle of the two spheres separated by 1 nm roughly the size of the R6G molecule. This situation is believed in SERS experiments from R6G molecule in silver colloidal solution where the molecule is trapped in between the colloidal particles termed as hot spots.[9,11] The polarization direction of the incident and scattered wave is taken along the dimer axis. Furthermore, in Raman scattering since there is only a small difference between the incident and scattered photon energies, we assume $\omega_i \approx \omega_s = \omega$. Therefore, from Eq. (2.43) we have

$$\frac{\sigma^{SERS}}{\sigma^{free}} \approx \left| \frac{\vec{E}(\vec{r},\omega)}{\vec{E}^0_{inc}(\vec{r},\omega)} \right|^4 = \left| F(\vec{k},\omega) \right|^2. \tag{3.1}$$

The enhancement (in log scale) calculated from Eqs. (3.1) and (2.41) is plotted as a function of the incident photon wavelength [Fig. 2(a)]. We find the maximum enhancement in the Raman cross section can reach more than ten orders of magnitude. For comparison, we have also calculated the SERS cross section from a molecule adsorbed on a single Ag sphere of radius 20 nm [Fig. 2(c)]. Note that even though scattering from a single sphere can be obtained from the solutions of the Maxwell equations directly, one can also use the same set of equations as derived in Sec. II. For a single sphere, however, the matrix B in Eq. (2.29) is a null matrix. The maximum enhancement in case of single sphere is about 5 orders of magnitude only and occurs around 360 nm. This peak corresponds to the excitation of the localized Mie mode of a single sphere that is given by the poles in the Mie scattering coefficient $c_{kl1\alpha}$ [Eq. (2.25)]. For $l=1$ and for small sphere radius, Mie mode is given by

$$\varepsilon(\omega) + 2 + \frac{12}{5}(kR)^2 \approx 0. \tag{3.2}$$

Note that the Mie resonance for a single metallic sphere occurs only for electrical mode ($\sigma=1$) and not for magnetic mode ($\sigma=2$).

Two broad peaks around 430 and 370 nm in case of dimer [Fig. 2(a)] correspond to the localized modes of the dimer. These modes of a coupled two sphere system have been discussed earlier by various authors using different techniques and approximations in the long wavelength ($kR \to 0$) limit.[24–26] For example, in Ref. 24, two spheres are treated as electrical point dipoles ($l=1$). The effects of higher partial waves are discussed approximately in Refs. 25 and 26. In our

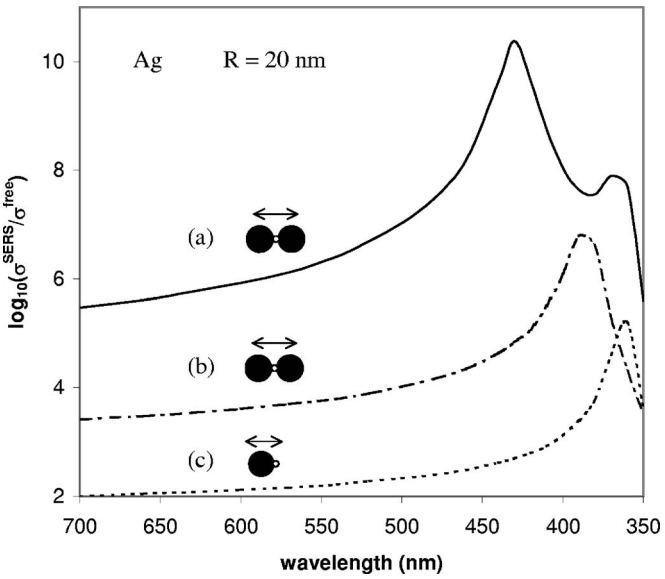

FIG. 2. Calculated electric field enhancements of Raman cross sections in the case of spherical silver particle cluster. (a) Molecule is adsorbed in between two spheres (dimer) each of radius $R=20$ nm. The full circle is a silver sphere and an open circle in between is a molecule of 1 nm size. The polarization of both incident and scattered photon is along dimer axis (shown by double arrow). (b) Same as in (a) but includes contributions of all partial waves only up to $l=1$ in Eq. (2.34). (c) Molecule is adsorbed on a single sphere of radius 20 nm at a distance of 0.5 nm.

theory, these long wavelength results can be obtained by retaining lowest partial wave contribution only in Eq. (2.32). These calculations are simple to carry out analytically and are useful for the analysis of our exact numerical results. For example, using $l=l'=1$ and $\sigma=\sigma'=1$ in Eq. (2.32), we have

$$B(1m1R_\alpha|1m'1R_\gamma) = 4\pi\sum_{l_1m_1} i^{-l_1}h_{l_1}^{(1)}(kd)y^*_{l_1m_1}(\Omega_{R_{\gamma\alpha}})g(\alpha|\gamma)C^{l_1m_1}_{1m1,1m'1}, \tag{3.3}$$

where $d=|\vec{R}_{\gamma\alpha}|$ is the distance between the centers of the two spheres. Note that the coefficients $C^{l_1m_1}_{1m1,1m'1}$ [see Eq. (A26)] are nonzero only for $l_1=0$ *and* 2 and for $m_1=m-m'$. In the long wavelength limit, that is, $kd\to 0$, we have

$$h_l^{(1)}(kd) \approx -i\frac{(2l-1)!!}{(kd)^{l+1}}. \tag{3.4}$$

Therefore, the dominant contribution in Eq. (3.3) comes from $l_1=2$ term only. Furthermore one can choose z axis of the polar coordinates along the dimer axis without loss of any generality. Therefore, $\Omega_{R_{\gamma\alpha}}=(0,\phi)$ and

$$y^*_{l_1m_1}(0,\phi) = \sqrt{\frac{2l_1+1}{4\pi}}\delta_{m_1,0}. \tag{3.5}$$

Thus in Eq. (3.3), only $l_1=2$ and $m_1=0$ term contributes in the summation. Thus we have

$$B(1m1R_\alpha|1m'1R_\gamma)c_{k11} = g(\alpha|\gamma)\frac{1-\varepsilon}{2+\varepsilon}\left(\frac{R}{d}\right)^3\sqrt{80\pi}C^{20}_{1m1,1m1}\delta_{mm'}, \tag{3.6}$$

where in the limit $kR\to 0$ we have used for the scattering Mie coefficients c_{k11} from Eq. (2.25) as

$$c_{k11} \approx -i\frac{2(1-\varepsilon)}{3(2+\varepsilon)}(kR)^3. \tag{3.7}$$

The Gaunt coefficients can also be calculated from Eq. (A26) as $C^{20}_{111,111}=C^{20}_{1-11,1-11}=1/\sqrt{80\pi}$ and $C^{20}_{101,101}=-2/\sqrt{80\pi}$. Thus the 6×6 matrix $[I\text{-}Bc]$ [Eq. (2.30)] reduces to the form:

$$[I-Bc] = \begin{pmatrix} I & \tau \\ \tau & I \end{pmatrix}, \tag{3.8}$$

where

$$\tau = \begin{pmatrix} -\Delta & 0 & 0 \\ 0 & 2\Delta & 0 \\ 0 & 0 & \Delta \end{pmatrix}, \tag{3.9}$$

$$\Delta = \frac{1-\varepsilon}{2+\varepsilon}\left(\frac{R}{d}\right)^3. \tag{3.10}$$

For a single sphere, for $l=1$, there are three degenerate Mie modes $(m=0,\pm 1)$. For two isolated spheres, there will be six degenerate modes for $l=1$. However, when the two spheres are brought closer, the degeneracy may be lifted because of dipole-dipole interaction. In Eq. (3.9), Δ essentially corresponds to this interaction. For isolated spheres $\Delta\to 0$ as $R/d\to 0$.

The eigenmodes of the coupled two spheres are given by $\mathrm{Det}[I\text{-}Bc]=0$. One can easily show that

$$\mathrm{Det}[I-Bc] = (1-\Delta)^2(1+\Delta)^2(1-2\Delta)(1+2\Delta) = 0. \tag{3.11}$$

Therefore, we now have two doubly degenerate modes for $\Delta=1$; $[\varepsilon(\omega)=(1-2\xi^3)/(1+\xi^3)]$ and $\Delta=-1$; $[\varepsilon(\omega)=(1+2\xi^3)/(1-\xi^3)]$. The nondegenerate modes are for $\Delta=1/2$; $[\varepsilon(\omega)=2(1-\xi^3)/(2+\xi^3)]$ and $\Delta=-1/2$; $[\varepsilon(\omega)=2(1+\xi^3)/(2-\xi^3)]$. The expressions in parenthesis where $\xi=d/R$ correspond to the value of $\varepsilon(\omega)$ obtained from Eq. (3.10) for the corresponding mode. The nondegenerate and degenerate modes correspond to the dipoles oscillating parallel $(m=0)$ and perpendicular $(m=\pm 1)$ to the dimer axis, respectively. These values agree exactly with the results of Refs. 24–26.

One can also calculate the scattered field due to the excitation of these modes by the incident EM wave from Eqs. (2.37) and (2.38). All modes may not be optical active. For example, $\tilde{B}$ is now 3×6 matrix. For the field in the middle of the two spheres, this is essentially same as B matrix except in Eq. (3.6), we now have $(2R/d)$ instead of R/d. Thus $\tilde{B}c=[8\tau\ 8\tau]$ where τ is 3×3 matrix defined in Eq. (3.9). The matrix $Q=[I-Bc]^{-1}$ can also be calculated easily from Eq. (3.8) and is of the form

$$Q = \begin{pmatrix} E & F \\ F & E \end{pmatrix}, \tag{3.12}$$

where E and F are 3×3 diagonal matrices with $E_{11}=E_{33}=1/(1-\Delta^2)$, $E_{22}=1/(1-4\Delta^2)$, $F_{11}=F_{33}=\Delta/(1-\Delta^2)$, and $F_{22}=-2\Delta/(1-4\Delta^2)$. Using these results in Eqs. (2.37) or (2.40), we have

$$\vec{E}_{sc}(\vec{r}\to 0,\omega) = \frac{-32\Delta}{1+2\Delta}\vec{E}^{\parallel}_{inc}(\omega) + \frac{16\Delta}{1-\Delta}\vec{E}^{\perp}_{inc}(\omega), \tag{3.13}$$

where

$$E^{\parallel}_{inc}(\omega) = -a^{inc}_{10}\hat{e}_0/\sqrt{6\pi}, \tag{3.14}$$

$$E^{\perp}_{inc}(\omega) = -(a^{inc}_{1-1}\hat{e}_{-1} + a^{inc}_{11}\hat{e}_1)/\sqrt{6\pi}, \tag{3.15}$$

are the components of the incident field parallel and perpendicular to the dimer axis, respectively. Close to the resonance, one can show that

$$E^{\parallel}_{sc}(\vec{r}\to 0,\omega) = i\frac{96(d/R)^3}{\varepsilon_2((d/R)^3-2)^2}E^{\parallel}_{inc}(\omega), \tag{3.16}$$

for $\Delta\approx -1/2$ and corresponds to the collective oscillations of the dipoles parallel to the dimer axis. For $\Delta\approx 1$, we have

$$E_{sc}^{\perp}(\vec{r}\to 0,\omega) = -i\frac{48(d/R)^3}{\varepsilon_2((d/R)^3+1)^2}E_{inc}^{\perp}(\omega), \quad (3.17)$$

and it corresponds to the collective motion perpendicular to the dimer axis. In Eqs. (3.16) and (3.17), ε_2 is the imaginary part of $\varepsilon=\varepsilon_1+i\varepsilon_2$. These results are also in agreement with those obtained in Ref. 29 using point dipole approximation for the spheres. For $d/R = 2.05$ used for our numerical results, the parallel mode has resonance for $\varepsilon_1(\omega) \approx -3$ and the enhanced field $|E_{sc}^{\parallel}/E_{inc}^{\parallel}| \approx 18.4/\varepsilon_2$. In Fig. 2(b), we have given the enhancement in the cross section for a dimer calculated from Eq. (2.41) retaining only $l=1$ partial wave. The maximum enhancement occurs around $\lambda = 390$ nm for $\varepsilon(\lambda=390\ \text{nm})=-3.9+0.20i$ slightly shifted towards longer wavelength due to finite sphere radius. For $\varepsilon_2 = 0.2$, the enhancement in Raman cross section $|E_{sc}^{\parallel}/E_{inc}^{\parallel}|^4 \approx 7\times 10^7$ in agreement with our numerical results in Fig. 2(b). For $d/R=2.05$, perpendicular mode has resonance for $\varepsilon_1(\omega)\approx -1.67$ and the enhanced scattered field $|E_{sc}^{\perp}/E_{inc}^{\perp}| \approx 4.5/\varepsilon_2$ is much smaller compared with that in the case of parallel mode. Note that, in Fig. 2(b), the incident and scattered fields are parallel to the dimer axis. Therefore, there is only one peak corresponding to the excitation of the parallel mode.

The effects of higher partial waves have been discussed in Refs. 25 and 26. One now has $2l_{\max}(l_{\max}+2)$ modes for two sphere cluster where $l_{\max}$ is the maximum number of partial waves considered in Eq. (2.30). The interaction between these multipolar modes has two effects:[25] (i) the parallel mode ($l=1$, $m=0$) discussed above shifts towards longer wavelengths, that is, from $\varepsilon(\omega)\approx -3$ to $\varepsilon(\omega)\approx -4$ and (ii) other modes corresponding to higher partial waves may become optical active, e.g., for $l=2$, $m=0$. Our exact numerical calculations support these results. For example, in Fig. 2(a), the peak at 390 nm in Fig. 2(b) shifts to 430 nm and another broad peak at 370 nm appears due to the excitation of the higher partial wave mode. However, at 430 nm, the enhancement in the cross section is almost two orders of magnitude more than at 370 nm. We also carried out calculations when the incident and scattered photon polarization is perpendicular to the dimer axis. However, the enhancement is much smaller in this case.[16]

In our numerical calculations, most of the contribution comes from the electrical mode ($\sigma=1$). The magnetic mode ($\sigma=2$) contribution is less than 1% because of the absence of the Mie resonance for this mode. Retaining only the electrical modes, the size of the matrix $[I-Bc]$ in Eq. (2.30) is $Nl_{\max}(l_{\max}+2)\times Nl_{\max}(l_{\max}+2)$ where N is the number of spheres in a cluster. $l_{\max}$ is the maximum value of the partial wave included in Eq. (2.30) to achieve convergence. In our calculations, we find the convergence within 2% for $l_{\max}=6$ (see Fig. 3). Even for three and four sphere clusters discussed later, convergence is within 3%. This is because in the calculations of the local modes of a cluster [poles of Q matrix Eq. (2.30)], the dominant contribution to the matrix elements of Bc comes from the poles of Mie coefficients (c_{kl1}) corresponding to lower partial waves only in the wavelength region considered here. The B matrix elements, however, are

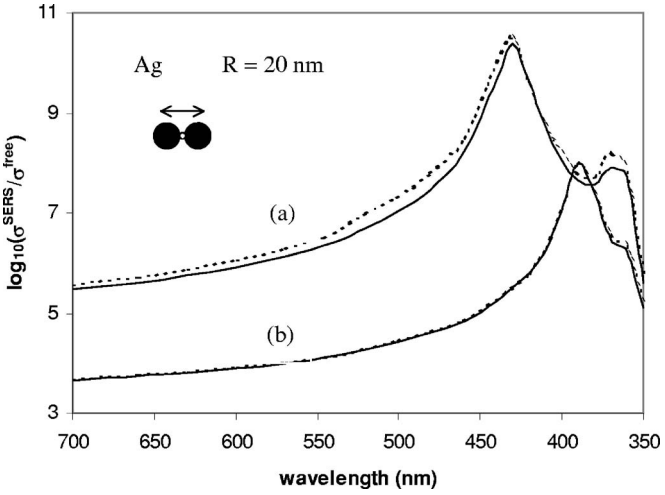

FIG. 3. Calculated electric field enhancement of Raman cross section for a dimer showing numerical convergence with the total number of partial waves included in Eq. (2.34) and particle separation. Full line is the result when all partial waves up to $l_{\max}=6$ are included. Dotted line is for $l_{\max}=7$. (a) For $d/R=2.05$ (b) $d/R=2.25$. Here d is the distance between the centers of two spheres and R is the sphere radius.

calculated exactly including all partial waves ($l_1 \le 12$) in the summation in Eq. (2.32). Far away from the Mie resonance region or for dielectric (nonmetal) spheres the convergence may be slow and one may need to include more partial waves in Eq. (2.30).

Another important reason for this convergence in our theory is that one can chose any point to be the origin of the spherical coordinate system because of the use of wave-vector space. By choosing the point where the field is calculated (position of the molecule) as the origin, one needs only $l=1$ and $\sigma=1$ term in Eq. (2.34). This is because in Eq. (2.34), $\vec{A}_{klm1}(\vec{r})$ contains $j_l(r)/r$ and for $r\to 0$, it is nonzero only for $l=1$. Note that $l=0$ term is not allowed in the summation. In this way, at least one summation ($lm\sigma$) in Eq. (2.34) is carried out exactly. In earlier work[29] that includes multiple scattering in real space, the center of coordinate system is taken as the center of one of the sphere in a cluster in order to use the addition theorem. Therefore, the above simplification cannot be used in order to calculate the field outside the spherical particle in a cluster and thus many more partial waves need to be included. In addition it has been found that convergence becomes even slower using real space with the increase of the ratio d/R where R is the radius of the sphere and d is the distance between the centers of the two spheres. In our theory, however, convergence becomes much better with increasing d/R because of the special choice of the origin. [See Figs. 3(b)].

In Fig. 4, we plot the maximum enhanced field due to the excitation of local modes as a function of the distance from the dimer and from a single sphere. The field at 430 nm is much more localized near a dimer compared with that from a single sphere at 360 nm. For example, the field decays with in 6 nm in case of dimer whereas it extends up to 25 nm for the sphere. This is usually the case in any metal particle cluster that the field is more localized near a cavity (cavity

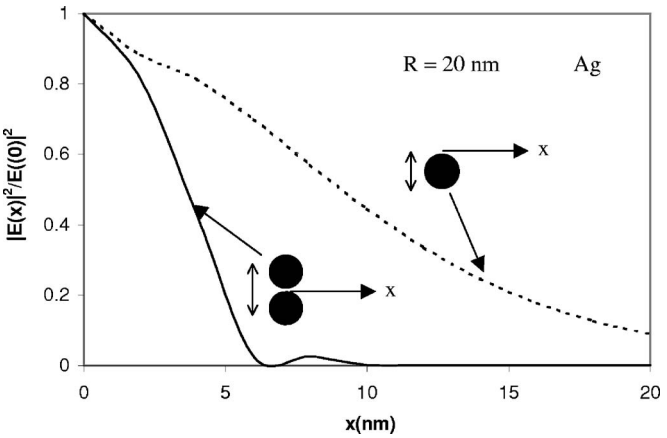

FIG. 4. Distance dependence of enhanced field due to local modes of a two-particle cluster and of a sphere. For dimer, $|\vec{E}(0)|^2/|\vec{E}_{inc}(0)|^2 \sim 1.6\times 10^5$ and occurs at $\lambda=430$ nm. For a single sphere, $|\vec{E}(0)|^2/|\vec{E}_{inc}(0)|^2 \sim 400$ at $\lambda=360$ nm. The polarization direction of the incident photon is also shown by the double arrow.

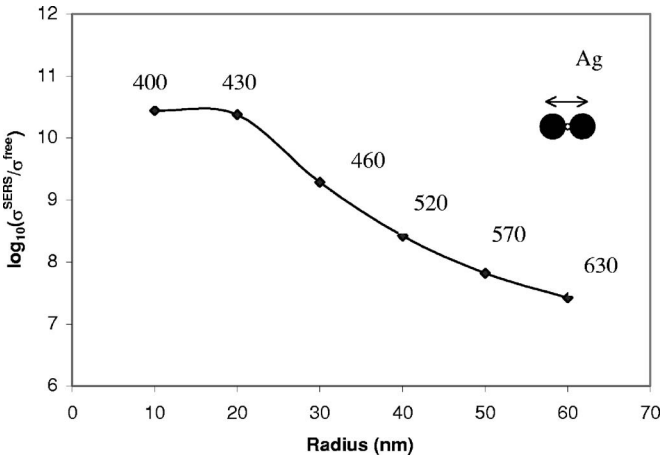

FIG. 5. Dependence of SERS cross section on the radius of spheres forming a dimer cluster. The numbers in the graph indicate the photon wavelength (in nm) for the maximum enhancement due to the resonant excitation of the local mode.

mode) and has very large electric field there.[17] As a result, the enhancement is much larger if the molecule is lying very near to the cavity. In Fig. 5, we have given the dependence of the maximum SERS enhancement on the radius of the spheres forming the dimer. The enhancement is maximum for sphere radius up to 20 nm and then decreases slowly. Also the local mode (peak) position shifts to a longer wavelength with the increasing sphere size. This is consistent with Eq. (3.2).

B. Three and four particles clusters

Next we consider clusters of three and four spherical particles with same radii of 20 nm. In Fig. 6, we have given the enhancement for a linear chain of three and four particles. The molecule of 1 nm size lies in between the two particles as shown in the figure. The case of dimer is also given for comparison. The polarization of the incident and scattered photon is along the chain. The maximum enhancement in the cross section is between 9 and 10 orders of magnitude somewhat less than in the case of dimer. However, there are now three broad peaks in the wavelength region considered here compared with two in the case of dimer. The peak at longer wavelength has dominant contribution coming from $l=1$ partial wave with some effects of higher partial waves. We find this peak shifts towards a longer wavelength as one goes from two to three to four particles chain. This trend is in agreement with the results obtained in dipole approximation of Ref. 24. For example, in Ref. 24, this peak corresponds to $\varepsilon=-3$ (dimer), $\varepsilon=-3.76$ (3 particle chain) and $\varepsilon=-4.32$ (4 particle chain) and corresponds to the collective motion of the dipoles along the chain. The other two peaks at 410 nm and at 370 nm correspond to higher partial waves. We find another important difference between the dimer and the linear chain cluster that there is now a sharp drop in the SERS enhancement near the first resonant peak in the case of linear chain. This behavior is independent of the position of the molecule. [See Figs. 6(c) and 6(d). Also see Fig. 8.] It shows this feature must be the result of sharp resonance mode structure of the chainlike cluster that may arise because of the interference effects due to higher partial waves included in our theory. Such features have been observed in SERS experiments from colloidal solutions.[42]

To understand these effects of higher partial waves, we consider a three particle chain in Fig. 7. When all partial waves up to $l_{max}=1$ are included in the summation in Eq. (2.34), there is only one peak at 410 nm (full line). This corresponds to the collective motion of all the dipoles along the chain in agreement with Ref. 24. Including all partial waves up to $l_{max}=2$, we find this peak moves towards a longer wavelength from 410 nm to 420 nm (dash line). Also

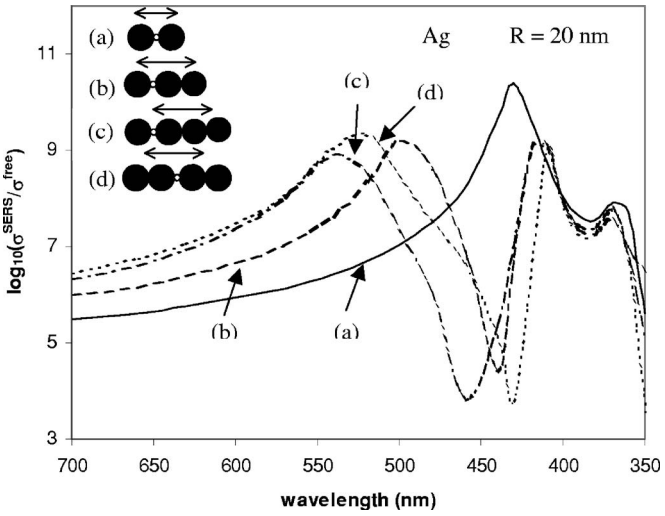

FIG. 6. Calculated electric field enhancement of Raman cross section from a molecule (open circle) of 1 nm size trapped in between a linear chain of two (full line), three (dashed line), and four silver particles. In the case of a four particle chain, both cases of molecule being trapped in the middle (dotted line) and between first and second particle (dash-dot line) are considered. Radius of each sphere is 20 nm. The polarization direction of both incident and scattered photon is along the chain.

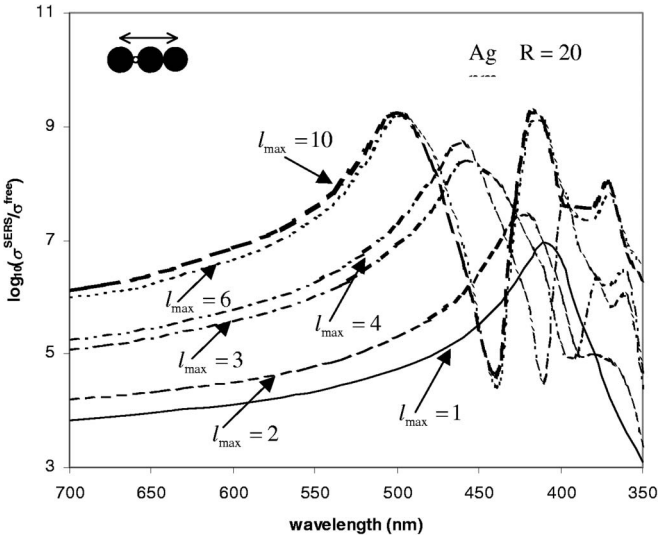

FIG. 7. Dependence of the resonance features of the electric field enhancement in case of a three particle chain on the maximum number of partial waves included in the summation in Eq. (2.34).

a second peak at 380 nm starts to develop. Including all partial waves up to $l_{max}=3$, the $l=1$ peak moves to 460 nm and the broad peak at 380 nm splits into two peaks at 380 nm and 360 nm (dash-dot line). Furthermore the SERS enhancement at 460 nm also increases giving a sharp resonance behavior. This trend continues when more partial waves are included making the resonance feature very sharp [$l_{max}=4$ (dash-dot), $l_{max}=6$ (dotted line), $l_{max}=10$ (thick dash line)]. This figure also shows the convergence results around $l_{max}=6$.

In Fig. 8, we consider a case where the molecule is lying on one end of the linear chain instead of being trapped in between the particles. We find the maximum enhancement to be much smaller (about 5 orders of magnitude only) roughly the same as in the case of a molecule adsorbed on a single sphere [see Fig. 2(c)]. However, the sharp resonance features are still present in case of a linear chain of three and four particles as in Fig. 6. This also shows that for maximum enhancement, the molecule must be trapped in between the particles in a cluster. This is consistent with our earlier results of Fig. 4 where the field is maximum localized inside the cavity near the cluster. Recently there is some interest to use silver nanorods with molecule lying on its tip for SERS experiments. However, our results of Fig. 8 representing some what of this structure indicates that a nanoscale rod with a molecule on its tip may not be the best structure for large SERS cross section.

In Fig. 9, we consider clusters of three and four particles in the triangular and square shape. The position of the molecule (open circle) and the polarization direction (double arrow) are shown in the inset. The enhancement in the cross section is between 9 and 10 orders of magnitude. In each case, there are 3 peaks in the wavelength region considered here. However, there is no sharp resonant feature as observed in the case of a linear chain cluster. The behavior is more like that of a dimer except now there is a third peak on the longer wavelength side giving less enhancement. This is evident

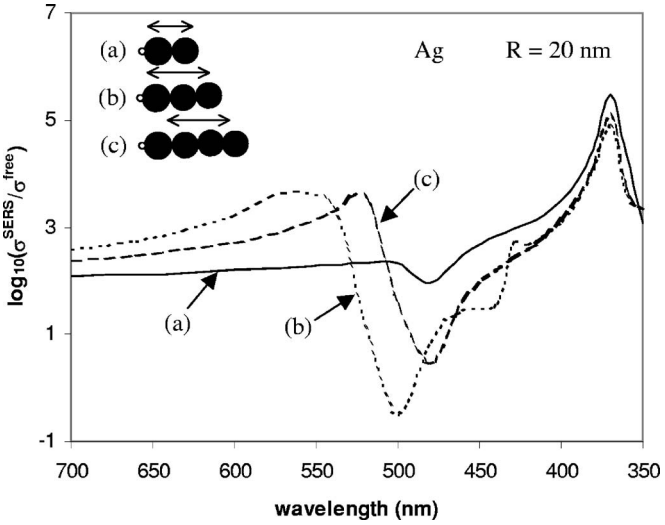

FIG. 8. Calculated electric field enhancement of Raman cross sections from a molecule of 1 nm size lying on one edge of a linear chain of two, three, and four silver particles. Radius of each sphere is 20 nm. The polarization direction of both incident and scattered photon is along the chain.

from Fig. 9(b) for an isosceles triangular shape cluster where the third particle is at 40 nm from the molecule and is not touching the other two spheres. This behavior with the main peak at 430 nm is similar to that of a dimer (dotted line). However, when the third particle comes closer at 34.5 nm forming an equilateral triangle [Fig. 9(a)], the main peak still remains at 430 nm, however, a third peak at 500 nm with enhancement up to 8 orders of magnitude develops (full line). In case of a square shape cluster [Fig. 9(c)], one has similar features except the third peak with similar enhance-

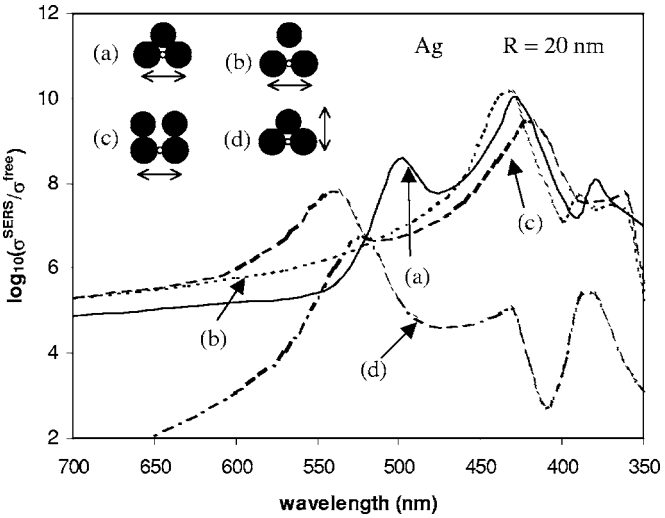

FIG. 9. Calculated electric field enhancement of Raman cross sections in the case of three and four silver particles cluster in the shape of an equilateral triangle [(a) and (d)], an isosceles triangle [(b)] and a square [(c)]. The molecule of 1 nm size is trapped between the two particles as shown in the inset. Radius of each sphere is 20 nm. The polarization direction of both incident and scattered photon is the same as shown by the double arrow.

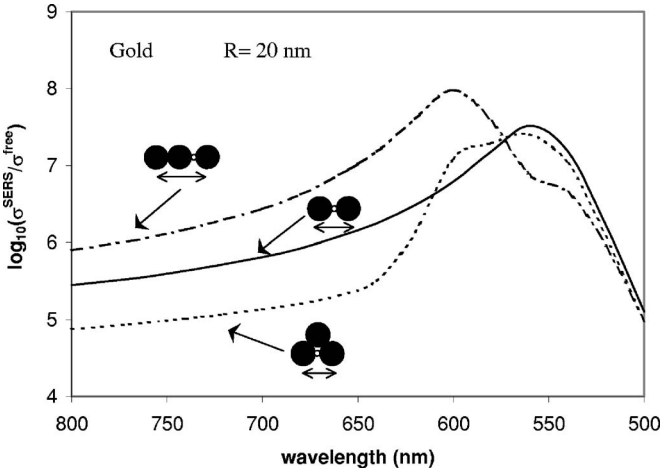

FIG. 10. Calculated electric field enhancement of Raman cross sections for two and three spherical gold particle clusters. Cluster size and molecule position is shown in the inset. The polarization direction of incident and scattered photon is the same and is shown by the double arrow.

ment now moves to 540 nm (dash line). In case of equilateral triangle, we have also considered the case when the photon polarization is perpendicular to its base [Fig. 9(d), dash dot line]. The enhancement decreases considerably, however, it is still large compared to that in the case of a dimer when photon polarization is perpendicular to the dimer axis.

In Fig. 10, we have given the enhancement calculated in the case of two and three gold particle clusters. We find the maximum enhancement of 8 orders of magnitude but in a broad wavelength range. There are no sharp peaks in the enhancement as seen in the case of silver particle clusters. These peaks are smeared out because of the large imaginary part of the dielectric function of gold. However, the broad maximum shifts towards longer wavelength with the increase in the number of particles in the cluster.

IV. CONCLUSIONS

In summary, we have developed an exact theory to calculate the enhanced electric field near a nanoparticle cluster of any shape or size. Our theory reproduces exactly the results obtained earlier for a dimer obtained in the dipole approximation ($l=1$).[24–26] However, we find in the case of these clusters, higher partial wave contribution is very important. This usually leads to more localization of the modes, shift modes towards longer wavelength and appearance of new modes those that can be excited optically. In the case of a linear chain cluster, we find an important new feature where the enhancement drops dramatically near the resonant peak indicating the existence of very localized modes for a chain. These sharp resonant features can be observed either in SERS or absorption experiments and may lead to information about the cluster size and shape responsible for large enhancements. The electric field contribution to the enhancement in SERS is found to be up to 10 orders of magnitude in the case of silver and is in a broad frequency range. The enhancement in the case of gold cluster is somewhat less but still much larger than in the case of a single gold spherical particle. We find a cluster in the shape of a linear chain of a few nanoparticles with a molecule trapped in between the particles gives the maximum enhancement. This is consistent with the experimental results of Ref. 9. The enhancement occurs in broad wavelength range and is always towards a longer wavelength side of the Mie mode of a single sphere. However, the enhancement for a linear chain is very sensitive to the photon polarization. For example, maximum enhancement occurs when both incident and scattered photon polarization directions are along the chain. There is almost no enhancement when polarization is perpendicular to the chain. On the other hand, in a triangular shape cluster, the enhancement is somewhat less but it is also less sensitive to the polarization direction. Furthermore, smaller particle size ($\leq$30 nm) in the cluster is preferred for maximum enhancement. The enhancement is maximum if the molecule is trapped very close to the cluster inside a cavity because of an extremely localized field there.

ACKNOWLEDGMENTS

I would like to acknowledge R. Bahuguna and L. Jusinski for many helpful discussions related to this work. I would also like to thank Rajesh Kumar Kommu for his help in writing the numerical program and for many helpful discussions. Part of this work was completed during my visit to the University of Missouri, Columbia in the summer of 2005. I thank S. Satpathy for making this visit possible and for many helpful discussions.

APPENDIX

Here we discuss the properties of the vector spherical harmonics following Refs. 36 and 38. Vector spherical harmonics are the result of coupling photon orbital angular momentum and its unit spin using relevant CG coefficients. Following Ref. 36, we define the vector spherical harmonics as

$$\vec{V}_{lLm}(\theta,\phi) = \sum_{\alpha=-1}^{1} \langle L1m-\alpha\alpha|lm\rangle y_{Lm-\alpha}(\theta,\phi)\hat{e}_\alpha, \quad \text{(A1)}$$

where

$$\hat{e}_1 = -\frac{1}{\sqrt{2}}(\hat{x}+i\hat{y}), \quad \hat{e}_0 = \hat{z}, \quad \hat{e}_{-1} = \frac{1}{\sqrt{2}}(\hat{x}-i\hat{y}), \quad \text{(A2)}$$

form an orthonormal set of three unit vectors, that is, $\hat{e}_m^* \cdot \hat{e}_{m'} = \delta_{mm'}$. For CG coefficients $\langle j_1 j_2 m_1 m_2 | jm\rangle$, we have used the notation of Ref. 43. For given l in Eq. (A1), L can take only three values, $l-1$, l, and $l+1$. Accordingly, we have a set of three vector spherical harmonics $\vec{V}_{ll-1m}(\Omega)$, $\vec{V}_{llm}(\Omega)$, and $\vec{V}_{ll+1m}(\Omega)$ which make a complete set of orthonormal functions

$$\int \vec{V}^*_{lLm}(\Omega) \cdot \vec{V}_{l'L'm'}(\Omega) d\Omega = \delta_{ll'}\delta_{LL'}\delta_{mm'}. \quad \text{(A3)}$$

This orthogonality condition can be easily verified using Eqs. (A1) and (A2) and the relation for the CG coefficients[43]

$$\sum_{\alpha=-1}^{1} \langle L1m-\alpha\alpha|lm\rangle\langle L1m-\alpha\alpha|l'm\rangle = \delta_{ll'}. \quad \text{(A4)}$$

For the discussions of eigensolutions $\vec{A}_{klm\sigma}(\vec{r})$ of the Maxwell equations, one constructs another set of three orthonormal functions by taking linear combination of $\vec{V}_{lLm}(\Omega)$ as

$$\vec{Y}_{lm1}(\Omega) = i\left[\left(\frac{l+1}{2l+1}\right)^{1/2}\vec{V}_{ll-1m}(\Omega) + \left(\frac{l}{2l+1}\right)^{1/2}\vec{V}_{ll+1m}(\Omega)\right]$$
$$= \hat{r}\times\vec{X}_{lm}(\Omega), \quad \text{(A5)}$$

$$\vec{Y}_{lm2}(\Omega) = \vec{V}_{llm}(\Omega) = \vec{X}_{lm}(\Omega), \quad \text{(A6)}$$

$$\vec{Y}_{lm3}(\Omega) = \left[\left(\frac{l}{2l+1}\right)^{1/2}\vec{V}_{ll-1m}(\Omega) - \left(\frac{l+1}{2l+1}\right)^{1/2}\vec{V}_{ll+1m}(\Omega)\right]$$
$$= \hat{r}y_{lm}(\Omega). \quad \text{(A7)}$$

The equality on the right hand side in these equations in terms of $\hat{r}\times\vec{X}_{lm}(\Omega)$, $\vec{X}_{lm}(\Omega)$, or $\hat{r}y_{lm}(\Omega)$ can be verified using the relevant expressions for the CG coefficients. In fact all vector spherical harmonics $\vec{V}_{lLm}(\Omega)$ [Eq. (A1)] involve the CG coefficients $\langle j_1 j_2 m_1 m_2|jm\rangle$ with $j_2=1$. These coefficients have simple analytical expressions[44] that make most of the calculations possibly analytically. Thus the two transverse functions $\vec{A}_{klm\sigma}(\vec{r})$ [Eqs. (2.7) and (2.8)] can be written as

$$\vec{A}_{klm1}(\vec{r}) = \left[\left(\frac{l}{2l+1}\right)^{1/2} f_{l+1}(kr)\vec{V}_{ll+1m}(\Omega) - \left(\frac{l+1}{2l+1}\right)^{1/2} f_{l-1}(kr)\vec{V}_{ll-1m}(\Omega)\right], \quad \text{(A8)}$$

$$\vec{A}_{klm2}(\vec{r}) = f_l(kr)\vec{V}_{llm}(\Omega). \quad \text{(A9)}$$

The result (A9) is straightforward. However, in deriving Eq. (A8), we have used the following recursion relations for the spherical Bessel functions $f_l(x)$:[36]

$$f_l'(x) + \frac{(l+1)}{x}f_l(x) = f_{l-1}(x), \quad \text{(A10)}$$

$$f_l'(x) - \frac{l}{x}f_l(x) = -f_{l+1}(x). \quad \text{(A11)}$$

Note that for $\sigma=1$ and 2, $\vec{A}_{klm\sigma}(\vec{r})$ and $\vec{Y}_{lm\sigma}(\Omega)$ are zero for $l=0$. The representation of $\vec{A}_{klm\sigma}(\vec{r})$ or $\vec{Y}_{lm\sigma}(\Omega)$ in terms of $\vec{V}_{lLm}(\Omega)$ makes some of the algebra simple especially for numerical purposes. For example

1. Fourier transformations of $\vec{A}_{klm\sigma}(\vec{r})$

From Eq. (2.10) we have

$$\vec{A}_{klm\sigma}(\vec{Q}) = \int d^3r e^{-i\vec{Q}\cdot\vec{r}}\vec{A}_{klm\sigma}(\vec{r}). \quad \text{(A12)}$$

Using the relation

$$e^{-i\vec{Q}\cdot\vec{r}} = 4\pi\sum_{lm}(-i)^l j_l(Qr)y_{lm}(\Omega_Q)y_{lm}^*(\Omega_r), \quad \text{(A13)}$$

and Eqs. (A8) and (A9) for $\vec{A}_{klm\sigma}(\vec{r})$ and the orthogonality relation for the spherical Bessel functions [Eq. (2.14)], one can easily show that

$$\vec{A}_{klm\sigma}(\vec{Q}) = 4\pi(-i)^l(-1)^\sigma\vec{Y}_{lm\sigma}(\Omega_Q)\frac{\pi}{2k^2}\delta(k-Q). \quad \text{(A14)}$$

2. Scattering t matrix for a single sphere

In Eq. (2.5), replacing $\overleftrightarrow{T}$ with $\overleftrightarrow{t}$, the scattered field (second term on its right hand side) from a single sphere of radius $R(\alpha)$ can be written as

$$\vec{E}_{sc}(\vec{r},\omega) = \int d^3r' d^3r'' \overleftrightarrow{d}^0(\vec{r}-\vec{r}',\omega)\cdot\overleftrightarrow{t}_\alpha(\vec{r}',\vec{r}'',\omega)\cdot\vec{E}_{inc}(\vec{r}'',\omega). \quad \text{(A15)}$$

In case, the center of the sphere lies on the origin of the coordinate system, for $\vec{E}_{inc}(\vec{r},\omega)=\vec{A}_{klm\sigma}(\vec{r})$, the scattered field $\vec{E}_{sc}(\vec{r},\omega)=c_{kl\sigma\alpha}\vec{A}_{klm\sigma}(\vec{r})$ where $c_{kl\sigma\alpha}$ are the Mie scattering coefficients. Using these results in Eq. (A15) and taking the Fourier transformations on both sides we obtain

$$c_{kl\sigma\alpha}\vec{Y}_{lm\sigma}(\Omega_k) = \frac{k}{4\pi i}\int d\Omega_{k'}\overleftrightarrow{t}_\alpha(\vec{k},\vec{k}',\omega)\cdot\vec{Y}_{lm\sigma}(\Omega_{k'}). \quad \text{(A16)}$$

In writing Eq. (A16), we have used Eqs. (A14) and (2.23) for $\vec{A}_{klm\sigma}(\vec{Q})$ and $\overleftrightarrow{d}^0(Q,\omega)$, respectively. Using the complete set property of $\vec{Y}_{lm\sigma}(\Omega_k)$, that is

$$\sum_{lm\sigma}\vec{Y}_{lm\sigma}(\Omega_k)\vec{Y}_{lm\sigma}^*(\Omega_{k'}) = \delta(\Omega_k-\Omega_{k'}), \quad \text{(A17)}$$

we obtain

$$\overleftrightarrow{t}_\alpha(\vec{k},\vec{k}',\omega) = \frac{4\pi i}{k}\sum_{lm\sigma}\vec{Y}_{lm\sigma}(\Omega_k)c_{kl\sigma\alpha}\vec{Y}_{lm\sigma}^*(\Omega_{k'}), \quad \text{(A18)}$$

where $|\vec{k}|=|\vec{k}'|=\sqrt{\varepsilon_0}\omega/c$.

3. Expansion of incident plane wave in terms of $\vec{A}_{klm\sigma}(\vec{r})$

Since $\vec{A}_{klm\sigma}(\vec{r})$ are the eigenfunctions of the Maxwell equation for the host medium, one can expand the incident plane wave in terms of this complete set as

$$\vec{E}_{inc}(\vec{r},\omega) = \vec{E}_{inc}(\vec{k},\omega)e^{i\vec{k}\cdot\vec{r}} = \sum_{lm\sigma}a_{klm\sigma}^{inc}(\vec{k})\vec{A}_{klm\sigma}(\vec{r}), \quad \text{(A19)}$$

where $a_{klm\sigma}^{inc}$ are the expansion coefficients. Multiplying both sides with $e^{-i\vec{Q}\cdot\vec{r}}$ and integrating with respect to $\vec{r}$, we obtain

$$(2\pi)^3\delta(\vec{k}-\vec{Q})\vec{E}_{inc}(\vec{k},\omega)=\sum_{lm\sigma}a^{inc}_{klm\sigma}(\vec{k})\vec{A}_{klm\sigma}(\vec{Q}). \tag{A20}$$

Using Eq. (A14) for $\vec{A}_{klm\sigma}(\vec{Q})$, multiplying both sides with $\vec{Y}^*_{lm\sigma}(\Omega_Q)$ and then integrating with respect to solid angle Ω_Q, we find

$$a^{inc}_{klm\sigma}(\vec{k})=4\pi i^l(-1)^\sigma\vec{E}_{inc}(\vec{k},\omega)\cdot\vec{Y}^*_{lm\sigma}(\Omega_k). \tag{A21}$$

For numerical purpose, it is convenient to use Eqs. (A5) and (A6) for $\vec{Y}^*_{lm\sigma}(\Omega_Q)$. For example

$$a^{inc}_{klm1}(\vec{k})=4\pi i^{l+1}\left[\left(\frac{l+1}{2l+1}\right)^{1/2}\vec{V}^*_{ll-1m}(\Omega_k)+\left(\frac{l}{2l+1}\right)^{1/2}\vec{V}^*_{ll+1m}(\Omega_k)\right]\cdot\vec{E}_{inc}(\vec{k},\omega), \tag{A22}$$

$$a^{inc}_{klm2}(\vec{k})=4\pi i^l\vec{V}^*_{llm}(\Omega_k)\cdot\vec{E}_{inc}(\vec{k},\omega). \tag{A23}$$

4. Gaunt coefficients $C^{l''m''}_{lm\sigma,l'm'\sigma'}$

From Eq. (2.33), we have

$$C^{l''m''}_{lm\sigma,l'm'\sigma'}=\int d\Omega\vec{Y}^*_{lm\sigma}(\Omega)\cdot\vec{Y}_{l'm'\sigma'}(\Omega)y_{l''m''}(\Omega), \tag{A24}$$

where $\vec{Y}_{lm1}(\Omega)=\hat{r}\times\vec{X}_{lm}(\Omega)$ and $\vec{Y}_{lm2}(\Omega)=\vec{X}_{lm}(\Omega)$ [Eqs. (A5) and (A6)]. Since $\hat{r}\times\vec{X}^*_{lm}(\Omega)\cdot\hat{r}\times\vec{X}_{lm}(\Omega)=\vec{X}^*_{lm}(\Omega)\cdot\vec{X}_{lm}(\Omega)$ [note $\hat{r}\cdot\vec{X}_{lm}(\Omega)=0$], one has $C^{l''m''}_{lm1,l'm'1}=C^{l''m''}_{lm2,l'm'2}$. For angular integration in Eq. (A24), we write $\vec{Y}_{lm2}(\Omega)$ in terms of $\vec{V}_{llm}(\Omega)$. Therefore, for $\sigma=\sigma'=1,2$, using Eqs. (A6) and (A1) in Eq. (A24), one has

$$C^{l''m''}_{lm\sigma,l'm'\sigma}=\sum_{\alpha=-1}^{1}\langle l1m-\alpha\alpha|lm\rangle\langle l'1m'-\alpha\alpha|l'm'\rangle\times\int y^*_{lm-\alpha}(\Omega)y_{l'm'-\alpha}(\Omega)y_{l''m''}(\Omega)d\Omega, \tag{A25}$$

where we have used $\hat{e}^*_\alpha\cdot\hat{e}_\beta=\delta_{\alpha\beta}$. The angular integration in Eq. (A25) can now be carried out using the addition of spherical harmonics.[43] We thus have

$$C^{l''m''}_{lm\sigma,l'm'\sigma}=\delta_{m,m'+m''}\left[\frac{(2l'+1)(2l''+1)}{4\pi(2l+1)}\right]^{1/2}\langle l'l''00|l0\rangle\sum_{\alpha=-1}^{1}\langle l1m-\alpha\alpha|lm\rangle\langle l'1m'-\alpha\alpha|l'm'\rangle\langle l'l''m'-\alpha m-m'|lm-\alpha\rangle. \tag{A26}$$

For $\sigma\neq\sigma'$, one can easily show that

$$C^{l''m''}_{lm2l'm'1}=-C^{l''m''}_{lm1l'm'2}. \tag{A27}$$

In this case, the angular integration in Eq. (A24) can also be carried out in a similar way using Eqs. (A5), (A6), and (A1). We have

$$C^{l''m''}_{lm1l'm'2}=-i\left[\frac{(2l'+1)(2l''+1)}{4\pi(2l+1)}\right]^{1/2}\sum_{\alpha=-1}^{1}\langle l'1m'-\alpha\alpha|l'm'\rangle\times\left[\begin{array}{l}\left(\frac{l}{2l+3}\right)^{1/2}\langle l+11m-\alpha\alpha|lm\rangle\langle l'l''m'-\alpha m''|l+1m-\alpha\rangle\langle l'l''00|l+10\rangle\\+\left(\frac{l+1}{2l+1}\right)^{1/2}\langle l-11m-\alpha\alpha|lm\rangle\langle l'l''m'-\alpha m''|l-1m-\alpha\rangle\langle l'l''00|l-10\rangle\end{array}\right]\delta_{m,m'+m''}. \tag{A28}$$

Equations (A26) and (A28) involve several CG coefficients. For numerical purpose, we have used the following relation to evaluate them:[45]

$$\langle j'j''m'm''|jm\rangle=\delta_{m,m'+m''}\sqrt{\frac{(j'+j''-j)!\,(j+j'-j'')!\,(j+j''-j')!\,(2j+1)}{(j+j'+j''+1)!}}\times\sum_k\frac{(-1)^k\sqrt{(j'+m')!\,(j'-m')!\,(j''+m'')!\,(j''-m'')!\,(j+m)!\,(j-m)!}}{k!\,(j'+j''-j-k)!\,(j'-m'-k)!\,(j''+m''-k)!\,(j-j''+m'+k)!\,(j-j'-m''+k)!}. \tag{A29}$$

[1] M. Fleischmann, P. J. Hendra, and A. J. McQuillan, Chem. Phys. Lett. **26**, 163 (1974).
[2] D. J. Jeanmaire and R. P. Van Duyne, J. Electroanal. Chem. Interfacial Electrochem. **84**, 1 (1977).
[3] M. G. Albrecht and A. Creighton, J. Am. Chem. Soc. **99**, 5215 (1977).
[4] A. Otto, in *Light Scattering in Solids IV*, edited by M. Cardona and G. Guntherodt (Springer-Verlag, Heidelberg, 1984).
[5] K. Arya and R. Zeyher, in *Light Scattering in Solids IV*, edited by M. Cardona and G. Guntherodt (Springer-Verlag, Heidelberg, 1984).
[6] M. Moskovits, Rev. Mod. Phys. **57**, 783 (1985).
[7] D.-S. Wang and M. Kerker, Phys. Rev. B **25**, 2433 (1982).
[8] K. Arya and R. Zeyher, Phys. Rev. B **24**, 1852 (1981).
[9] S. Nie and S. R. Emory, Science **275**, 1102 (1997).
[10] J. T. KrugII, G. D. Wang, S. R. Emory, and S. Nie, J. Am. Chem. Soc. **121**, 9208 (1999).
[11] K. Kneipp, H. Kneipp, I. Itzkan, R. R. Dasari, and M. S. Feed, Chem. Rev. (Washington, D.C.) **99**, 2957 (1999).
[12] K. Kneipp, Y. Wang, H. Kneipp, L. T. Perelman, I. Itzkan, R. R. Dasari, and M. S. Feld, Phys. Rev. Lett. **78**, 1667 (1997).
[13] K. Kneipp, H. Kneipp, V. B. Kartha, R. Manoharan, G. Deinum, I. Itzkan, R. R. Dasari, and M. S. Feld, Phys. Rev. E **57**, R6281 (1998).
[14] A. M. Michaels, M. Nirmal, and L. E. Brus, J. Am. Chem. Soc. **121**, 9932 (1999).
[15] A. M. Michaels, J. Jiang, and L. Brus, J. Phys. Chem. B **104**, 11965 (2000).
[16] H. Xu, E. J. Bjerneld, M. Kall, and L. Borjesson, Phys. Rev. Lett. **83**, 4357 (1999).
[17] H. Xu, J. Aizpurua, M. Kall, and P. Apell, Phys. Rev. E **62**, 4318 (2000).
[18] H. Lin, J. Mock, D. Smith, T. Gao, and M. J. Sailor, J. Phys. Chem. B **108**, 11654 (2004).
[19] K. Arya, Proc. SPIE **5703**, 9 (2005).
[20] M. Futamata, Y. Maruyama, and M. Ishikawa, J. Phys. Chem. B **108**, 13119 (2004).
[21] M. A. Young, D. A. Stuart, O. Lyandres, M. R. Glucksberg, and R. P. Van Duyane, Can. J. Chem. **82**, 1435 (2004).
[22] D. H. Jeong, Y. X. Zhang, and M. Moskovits, J. Phys. Chem. B **108**, 12724 (2004).
[23] J. D. Jackson, *Classical Electrodynamics*, 3rd ed. (Wiley, New York, 1998), Chap. 9.
[24] P. Clippe and R. Evrard, Phys. Rev. B **14**, 1715 (1976).
[25] R. Ruppin, Phys. Rev. B **26**, 3440 (1982).
[26] M. Schmeits and L. Dambly, Phys. Rev. B **44**, 12706 (1991).
[27] N. Zabala, A. Rivacoba, and P. M. Echenique, Phys. Rev. B **56**, 7623 (1997).
[28] F. J. Garcia de Abajo and J. Aizpurua, Phys. Rev. B **56**, 15873 (1997).
[29] M. Inoue and K. Ohtaka, J. Phys. Soc. Jpn. **52**, 3853 (1983).
[30] J. H. Bruning and Y. T. Lo, IEEE Trans. Antennas Propag. **19**, 378 (1971).
[31] S. Stein, Q. Appl. Math. **19**, 15 (1961).
[32] O. R. Cruzan, Q. Appl. Math. **20**, 33 (1962).
[33] V. A. Davis and L. Schwartz, Phys. Rev. B **31**, 5155 (1985).
[34] K. Arya, Z. B. Su, and J. L. Birman, in *Scattering and Localization of Classical waves in Random media*, edited by P. Sheng (World Scientific, Singapore, 1990).
[35] R. G. Barrera and R. Fuchs, Phys. Rev. B **52**, 3256 (1995).
[36] G. B. Arfikin and H. J. Weber, *Mathematical Methods for Physicists*, 5th ed. (Academic Press, New York, 2001), Chap. 12.
[37] E. L. Hill, Am. J. Phys. **22**, 211 (1954).
[38] J. M. Blatt and V. Weisskopf, *Theory of Nuclear Physics* (Wiley, New York, 1952), Appendix B and Chap. 12.
[39] R. Ruppin and R. Englman, J. Phys. C **1**, 631 (1968).
[40] P. B. Johnson and R. W. Christy, Phys. Rev. B **6**, 4370 (1972).
[41] H. Raether, *Surface Plasmons on Smooth and Rough Surfaces and on Gratings*, Springer Tracts in Modern Physics, Vol. 111 (Springer, Verlag, 1988).
[42] R. P. Van Duyne (private communication).
[43] A. Messiah, *Quantum Mechanics*, Vol. II (North-Holland, Amsterdam, 1965), Appendix C.
[44] E. U. Condon and G. H. Shortley, *The Theory of Atomic Spectra* (Cambridge University, Cambridge, 1963), Chap. 3.
[45] D. Zwillinger, *Standard Mathematical Tables and Formulae*, 30th ed. (CRC Press, New York, 1996), p. 527.